MinEx CRC Limited
26 Dick Perry Avenue, Kensington, WA, 6151
PO Box 1130, Bentley, WA, 6102, Australia
admin@minexcrc.com.au

ABN: 66 625 533 913

MinEx CRC provides financial support to the value of $1K to promote Honours and Masters by Coursework projects that are aligned with the mission of MinEx CRC and to encourage young researchers toward a career in mineral exploration research. Projects are not restricted to MinEx CRC Participants and Affiliates.

Please note that the content of this thesis has not been subjected to peer-review and subsequent corrections.

Australian Government
Department of Industry, Science and Resources
Cooperative Research Centres Program

LONDON'S GLOBAL UNIVERSITY

CENG0037 MSc Research Project

Apatite chemistry for copper discovery in northern Queensland, Australia

by:

Yirong SUN

Student's registration number: 23030304

Supervisor(s): Caroline Tiddy

Travis Batch

Adrienne Brotodewo

A thesis submitted to the University of London for the degree of Master of Science

Department of Chemical Engineering

University College London (UCL)

September 2023

Declaration

I, Yirong SUN, confirm that the work presented in this thesis is my own.

Where information has been derived from other sources, I confirm that this has been indicated in the thesis.

Word count: 4563

(excluding the title page, table of contents, references, tables, figures and appendices)

Has the written report been submitted on Moodle? Yes / No

Have relevant source codes and/or raw data been submitted on Moodle? Yes / No

Has the lab space used been cleaned up (if applicable)? Yes / No

Yirong SUN	Yirong SUN	26/08/2024
.....	.....	.....
Student's Name	Student's Signature	Date

TABLE OF CONTENTS

ABSTRACT

This study explores the application of apatite mineral chemistry in exploring for iron sulfide-copper-gold (ISCG) mineral deposits. The study uses the Jericho ISCG deposit in the Cloncurry region of Queensland, Australia as a case study area. Detailed scanning electron microscopy (SEM) imaging and chondrite-normalised trace element profiles obtained through laser ablation inductively coupled plasma mass spectrometry (LA-ICP-MS) are used to characterise apatite grains from barren and mineralised samples. These methods allow for the precise characterisation of apatite grains, revealing subtle variations in their chemical composition that reflect their formation and alteration histories. The geochemical patterns observed are compared with established studies to assess the potential metamorphic origins of the samples. The study demonstrates that the chemistry of apatite from baren and mineralised samples can be distinguished based on rare earth element ratios, namely La/Lu versus La/Sm, and can be used to develop effective strategies for exploration and characterisation of key mineral resources. These findings have significant implications for sustainable development, particularly in securing the mineral resources crucial for the global transition to renewable energy.

INTRODUCTION

As the world strives to achieve net-zero emissions by 2050, there is a major shift from fossil fuel power to renewable energy generation (Anika et al., 2022). This transition requires a dramatic increase in the production and deployment of green technologies such as solar panels, wind turbines, and electric vehicles (Chen et al., 2019) that rely heavily on critical minerals such as copper. This reliance is resulting in increasing global demand of copper such that a significant shortfall in supply is anticipated by as early as 2030 (S&P Global, 2022).

Supply of copper may be appeased through discovery of new mineral deposits (Mudd and Jowitt, 2018). However, discovery is becoming increasingly challenging as most ore-bearing rocks are buried under young, barren rock formations, making traditional exploration methods less effective (Kelley et al., 2006). These challenges are driving the need for innovative exploration techniques that can locate hidden deposits more accurately and efficiently. One such technique is using the chemical properties of minerals such as zircon, monazite and apatite that may indicate proximity to mineralisation (McClenaghan, 2005; Mao et al., 2016; Brotodewo et al., 2021; Tiddy et al., 2021).

Apatite can contain various trace elements such as rare earth elements (REEs), uranium, and thorium, which can be used to trace the origin and evolution of mineralised hydrothermal fluids (Mao et al., 2016; Andersson et al., 2019). Apatite has been successfully used in exploration for commodities including orogenic gold (Zhang et al., 2020) and porphyry copper deposits (Bouzari et al., 2016). Despite progress, there are still major gaps in our understanding of how apatite can be used to locate specific types of deposits. For example, there is little understanding on using apatite to find iron sulfide-copper-gold (ISCG) deposits.

This dissertation aims to determine whether the chemistry of the mineral apatite can be used as an indicator of ISCG mineralisation using the Jericho ISCG deposit in the Cloncurry District, north-west Queensland as a case study area. Apatite grains were imaged using a scanning electron microscope (SEM) and their chemistry determined using laser ablation inductively

coupled plasma mass spectrometry (LA-ICP-MS). Results were compared with global apatite chemistry from known deposits to identify characteristics and trends associated with mineralisation. The findings are discussed in the context of ISCG mineral exploration to support the global net zero emissions targets.

BACKGROUND

Apatite

Apatite is a group of phosphate minerals that includes fluorapatite, chlorapatite, and hydroxyapatite (McConnell, 2012). These minerals share a general chemical formula of $Ca_5(PO_4)_3(F, Cl, OH)$, where the anion group can vary. Apatite typically forms in hexagonal crystals that are often well-defined and can be prismatic or tabular in habit, often displaying striations along the prism faces (Rakovan, 2002; Ptáček, 2016). The crystals can exhibit a variety of colours, including green, yellow, blue, and violet, depending on the impurities present (Ptáček, 2016). With a hardness of 5 on the Mohs scale, apatite is relatively soft compared to other minerals, making it more susceptible to scratching (Ptáček, 2016). Apatite is known for its glassy to vitreous lustre and white streak (Ptáček, 2016).

Apatite is a common mineral found in many different types of rocks, including igneous, metamorphic, and sedimentary (Bouzari et al., 2016) and is commonly used for U-Pb dating (Chew et al., 2011; Thomson et al., 2012). Apatite can incorporate elements such as REEs, U, Th, Sr and S into its crystal lattice, making it valuable for providing insights into the types of hydrothermal fluids and conditions that led to deposit formation (Belousova et al., 2002; Bruand et al., 2017). Apatite is a crucial mineral in the exploration and identification of ore deposits due to its ability to incorporate various trace elements into its crystal structure. Apatite can be found in economic amounts within hydrothermal veins (Mitsis and Economou-Eliopoulos, 2001) and is common in uneconomic proportions in several types of mineral deposits including IOCG deposits, skarn deposits, and porphyry Cu-Au deposits. In IOCG systems, apatite often forms as a primary or secondary mineral, enriched with REEs and other trace elements such as Sr, U, Th, Pb (Simon et al., 2018). Skarn deposits, formed by the contact metamorphism of carbonate rocks near igneous intrusions, contain apatite associated with ore minerals like tungsten, copper, gold, and iron (Adlakha et al., 2018). In porphyry deposits, apatite occurs as an accessory mineral, reflecting ore formation conditions (Xie et al., 2018). Apatite also forms in hydrothermal alteration zones, where mineral-rich fluids introduce and concentrate metals, and in magmatic environments, where it crystallises from magma, incorporating trace elements linked to primary magmatic ore deposits (Piccoli and Candela, 2002).

The chemistry of apatite can be used in used as an indicator towards mineralisation (Belousova et al., 2002; Mao et al., 2016). For example, trace elements like REEs, Sr, U and Th in apatite can indicate the presence of IOCG and skarn deposits (Mao et al., 2016). Analysing the chemical composition of apatite can help geologists identify potential mineralised zones and guide exploration efforts (Kelley et al., 2006). This makes apatite chemistry an invaluable tool for both discovering new ore deposits and gaining insights into the formation of existing ones.

Jericho ISCG deposit

The case study used in this study is the Jericho ISCG deposit, which is located in the Cloncurry District of north-west Queensland, Australia, in the easternmost region of the Mount Isa Inlier (Fig. 1)

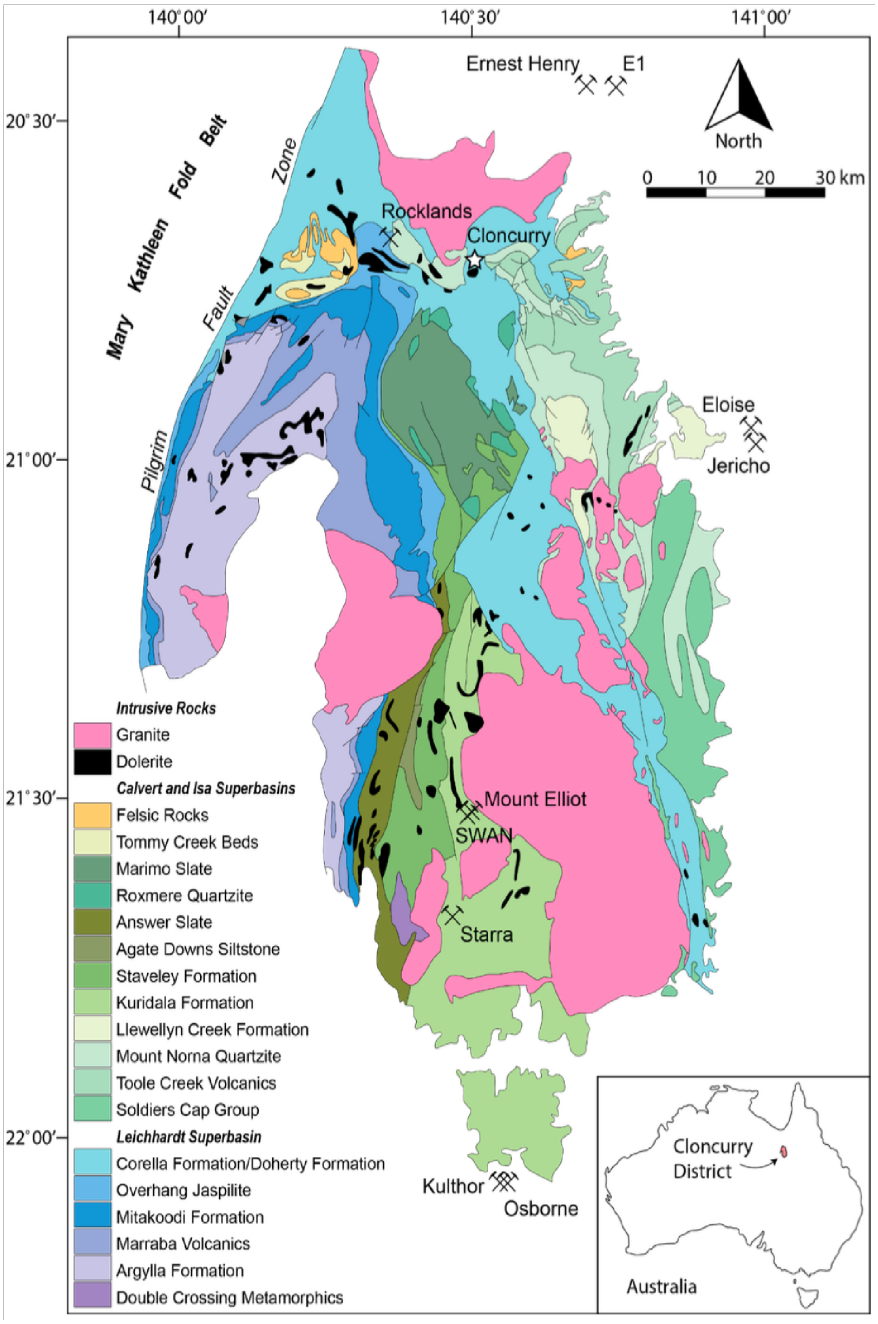

Figure 1. Geology of the Cloncurry District, Queensland, Australia, showing the locations of significant IOCG and ISCG mineral deposits, including the Jericho deposit. From the manuscript by Batch et al. (in review).

This area, bound by the Pilgrim Fault Zone to the west and extending eastward to include Paleoproterozoic sequences beneath younger geological cover, is renowned for its extensive mineralisation. The Cloncurry District is a prospective area for various types of ore deposits, including IOCG and ISCG, as well as Broken Hill-type lead-zinc-silver (Pb-Zn-Ag) mineralisation

(Walters and Bailey, 1998). The Cloncurry District is home to numerous world-class deposits, highlighting its importance for mining and exploration.

The Mount Isa Inlier comprises rocks aged from 1.8 to 1.5 billion years old and has undergone a complex geological history of significant folding, faulting, and metamorphism that are vital for forming mineral deposits. The Mt Isa Inlier comprises metamorphosed sedimentary and volcanic rocks, interspersed with intrusive igneous rocks. It hosts the Leichhardt, Calvert, and Isa Superbasins, primarily composed of meta-sedimentary units (Betts et al., 2006). Extensive greenschist to amphibolite facies metamorphism has transformed the rocks, aiding mineral deposit formation (Foster and Rubenach, 2006). Numerous granites and pegmatites intrude preexisting rocks. Events such as faulting and fracturing, folding, igneous activity during key deformation phases created pathways for mineralising fluids, allowing mineralisation to be concentrated within existing structures (Case et al., 2018).

The Cloncurry District has undergone multiple phases of tectonic activity, including compression, extension, and shearing, which have created pathways for hydrothermal fluids and facilitated the emplacement of mineral deposits (Rubenach et al., 2008). The region's complex metamorphic history, along with episodes of magmatism, has played a crucial role in the remobilisation and concentration of metals, leading to the formation of economically significant deposits like Jericho. Hydrothermal fluids, driven by magmatic and tectonic processes, have extensively interacted with the host rocks, resulting in the deposition of sulfide minerals.

The Jericho deposit, situated about 60 km southeast of the Cloncurry township and adjacent to the north-south oriented Levuka Shear Zone, hosts ISCG mineralisation. This mineralisation predominantly occurs in metamorphosed sedimentary rocks, such as psammite and psammopelite, within the Mount Norna Quartzite of the Soldiers Cap Group (Minotaur Exploration, 2020). The deposit features west-dipping massive chalcopyrite-pyrrhotite replacement lodes and veins formed within extensional fracture networks (Minotaur Exploration, 2019). Mineralisation consists of chalcopyrite overprinting earlier pyrrhotite, with higher concentrations of mineralisation found around precursor quartz veins (Baker, 1998). Hydrothermal alteration at Jericho is limited and primarily consists of centimetre scale biotite alteration, which is not as extensive as that found in other regional deposits (Batch et al., in Review).

METHODOLOGY

Sample selection and preparation

Samples were selected based on their association with mineralisation and apatite content. Drill hole EL18D18 was used as it intersects mineralisation at Jericho.

Samples were sent to Geotrack Laboratories in Melbourne, Australia for apatite separation using standard heavy liquid techniques. Apatite was mounted in one inch epoxy resin discs as individual grains or grains within rock chips.

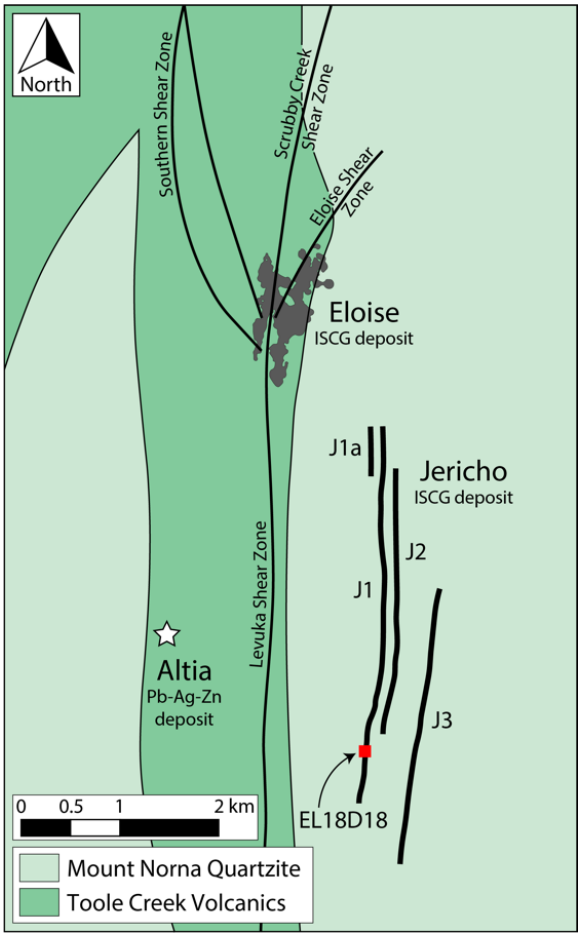

Figure 2. Simplified geological map showing the location of the Jericho ISCG deposit and drillhole EL18D18 used in this study. The location of the Jericho deposit is also shown in Figure 1. Map taken from Batch et al. (in review).

Scanning Electron Microscope (SEM)

All sample SEM images presented in this paper were taken with the Zeiss Merlin FEG SEM and were acquired at the University of South Australia. SEM images were obtained with a backscatter electron (BSE) detector. The SEM imaging conditions were fixed with the accelerating voltage was set to 20 kV, working distance set to 10 mm and the probe current set to 3 nA. All electron dispersive spectroscopy (EDS) maps were acquired with a pixel dwell time of 100 µs.

LA-ICP-MS

The trace and REE chemistry of apatite was analysed at the Future Industries Institute of the University of South Australia using LA-ICP-MS. Samples for LA-ICPMS were ablated using a Teledyne-Cetac Iridia nanosecond ArF 193nm Excimer, equipped with a cobalt sample cell, connected to an Agilent 8900 triple quad ICP-MS via flexible tubing. The method used for the LA-ICP-MS analysis of two apatite samples from the Jericho area in this work was adopted from that reported by Thompson et al. (2018) for similar analyses. The laser was operated at a wavelength of 193 nm with a repetition rate of 5 Hz, delivering 300 laser shots per minute. The background measurement was recorded for 60 seconds, followed by 60 seconds of sample analysis, with a fluence of 4 J/cm^2. For the ICP-MS, the Agilent 8900 was utilised with an RF power of 1450W, and an argon auxiliary gas flow rate of 0.90 L/min. The comprehensive

list of analysed elements and their corresponding isotopes includes: ^{23}Na, ^{24}Mg, ^{28}Si, ^{29}Si, ^{31}P, ^{34}S, ^{35}Cl, ^{39}K, ^{43}Ca, ^{44}Ca, ^{47}Ti, ^{49}Ti, ^{51}V, ^{55}Mn, ^{56}Fe, ^{63}Cu, ^{66}Zn, ^{75}As, ^{85}Rb, ^{88}Sr, ^{89}Y, ^{90}Zr, ^{93}Nb, ^{95}Mo, ^{137}Ba, ^{139}La, ^{140}Ce, ^{141}Pr, ^{146}Nd, ^{147}Sm, ^{153}Eu, ^{157}Gd, ^{159}Tb, ^{163}Dy, ^{165}Ho, ^{166}Er, ^{169}Tm, ^{172}Yb, ^{175}Lu, ^{206}Pb, ^{207}Pb, ^{208}Pb, ^{232}Th, ^{238}U. Raw counts per second (cps) data from individual spots were processed using iolite software to calculate element concentrations in parts per million (ppm) using ^{43}Ca as an internal standard.

RESULTS

Sample descriptions

Two samples from drill hole EL18D18 (Fig. 2) were selected from the Jericho area at depths of 113.8 m and 123.0 m. Both samples are psammite with a dominant mineralogy of quartz, feldspar and biotite. Sample EL18D18_113.3m was taken from within mineralisation and contains abundant sulfides dominated by pyrite and chalcopyrite (~25% of the whole rock). Sample EL18D18_123.0m was taken from an unmineralised area and contains minor sulfides (<1% of the whole rock).

Apatite SEM analysis

Sample EL18D18_113.3m (Fig. 3a-c) preserves large apatite that display variable textures from areas that are fractured and have a complex texture with irregular shapes (Fig. 3a) to large, inclusion-free grains with relatively smooth edges, a predominantly a uniform grey consistent with a homogeneous BSE response, with a regular geometry (Fig. 3a-c). Apatite can be rimmed by a mineral with a bright BSE response and that is rich in REE and P from EDS chemistry, suggesting it is rhabdophane (Fig. 3a). Some apatite grains contain inclusions. EDS spot chemistry shows that these inclusions can be Fe- and S- rich, with some also containing Cu, and are therefore likely pyrite and chalcopyrite (Fig. 3b, c).

Sample EL18D18_123.0m (Fig. 3d-f) preserves apatite grains with an irregular flake structure with edges that appear relatively irregular and slightly jagged or fragmented and occurring with biotite and quartz (Fig. 3d) or as inclusions within biotite (Fig. 3e, f). Grains are mostly roughly circular in shape (Fig. 3d, e) with some grains being predominantly composed of multiple elongated lamellar structures, arranged in a narrow and elongated equant shape (Fig. 3f).

EL18D18_113.3m EL18D18_123.0m

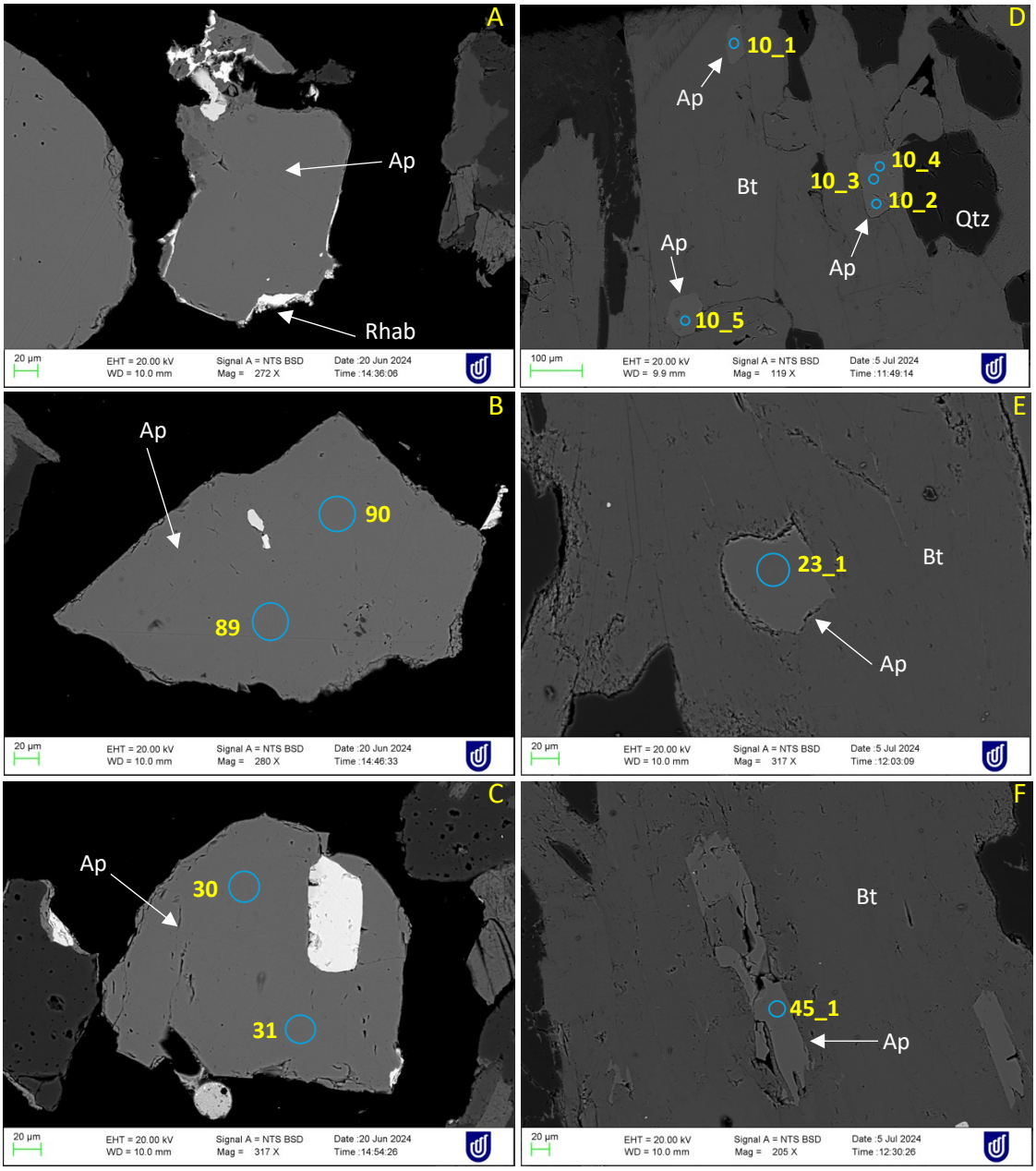

Figure 3. Representative SEM images of apatite for selected samples from drill hole EL18D18 in the Jericho area. Drill hole location is shown in Figure 2. (a) Apatite rimmed by rhabdophane, sample EL18D18_113.3m; (b) Apatite within small inclusions (?sulfides), sample EL18D18_113.3m; (c) Apatite with large inclusion of chalcopyrite (bright BSE response), sample EL18D18_113.3m; (d) Apatite grains within biotite, sample EL18D18_123.0m; (e) Apatite within biotite, sample EL18D18_123.0m; (f) Elongate apatite grain within biotite, sample EL18D18_123.0m. Mineral abbreviations: Ap: apatite; Rhab: rhabdophane; Bt: biotite; Qtz: quartz. Blue circles with yellow numbers indicate locations of LA-ICP-MS analysis points.

Apatite chemistry

Table 1: Representative LA-ICP-MS analysis results of apatite sample EL18D18 from the Jericho deposit. Drill hole location is shown in Figure 2. Data in is parts per million (ppm). b.d.l. = below detection limit. All data is given in Supplementary Material.

Sample ID	EL18D18_113.3m	EL18D18_113.3m	EL18D18_113.3m	EL18D18_123.0m	EL18D18_123.0m	EL18D18_123.0m
Site #	56	68	72	10_3	23_1	33_1
Type	Group 1	Group 1	Group 2	Group 3	Group 3	Group 3
^{23}Na	127.49	162.35	119.49	40.86	670.29	39.73
^{24}Mg	39.67	22.08	9.04	30.06	45499	34.49
^{28}Si	678.27	526.68	343.49	416.15	158290	508.53
^{29}Si	800.48	675.56	449.3	532.95	117032	570.81
^{31}P	242588	242401	241969	231076	270742	264502
^{34}S	b.d.l.	b.d.l.	b.d.l.	b.d.l.	372.55	193.28
^{35}Cl	b.d.l.	507.42	475.1	1845.09	9362.42	5357.85
^{39}K	b.d.l.	7.28	b.d.l.	b.d.l.	80497	b.d.l.
^{44}Ca	404093	411662	400943	405000	395424	397900
^{47}Ti	11.22	20.25	14.96	13.97	10589	11.25
^{49}Ti	b.d.l.	b.d.l.	b.d.l.	b.d.l.	15149	b.d.l.
^{51}V	0.39	0.44	b.d.l.	0.44	378.17	0.42
^{55}Mn	162.43	160.72	146.62	334.68	1329.35	365.71
^{56}Fe	283.99	171.61	58.08	305.61	150570	374.96
^{63}Cu	b.d.l.	b.d.l.	b.d.l.	b.d.l.	b.d.l.	b.d.l.
^{66}Zn	b.d.l.	b.d.l.	b.d.l.	b.d.l.	90.42	b.d.l.
^{75}As	38.36	19.56	1.42	14.72	16.57	12.84
^{85}Rb	0.15	b.d.l.	b.d.l.	b.d.l.	804.07	0.13
^{88}Sr	108.3	126.93	162.26	162.1	169.95	183.05
^{89}Y	1014.99	705.7	403.75	204.64	208.51	218.96
^{90}Zr	0.06	b.d.l.	b.d.l.	b.d.l.	0.45	b.d.l.
^{93}Nb	b.d.l.	0.03	b.d.l.	b.d.l.	7.13	b.d.l.
^{95}Mo	b.d.l.	b.d.l.	b.d.l.	b.d.l.	b.d.l.	b.d.l.
^{137}Ba	0.15	2.4	0.24	0.32	982.48	0.46
^{139}La	44.83	16.21	24.87	32.78	38.26	53.97
^{140}Ce	143.9	59.69	87.95	99.38	109.76	166.38
^{141}Pr	23.44	11.09	15.9	14.13	16.88	25.66
^{146}Nd	122.57	67.32	103.95	75.91	85.48	129.23
^{147}Sm	55.67	37.72	58.87	27.26	30.33	40.18
^{153}Eu	10.57	8.52	13.2	5.38	6.02	8.06
^{157}Gd	107.03	76.84	144	40.74	42.11	49.38
^{159}Tb	20.52	14.8	24.35	6.01	6.05	6.7
^{163}Dy	152.69	106.55	132.87	34.8	36.29	37.83
^{165}Ho	33.24	23.24	17.04	6.92	7.09	7.48
^{166}Er	93.95	66.14	28.31	20.02	20.54	21.58
^{169}Tm	12.34	8.46	2.26	2.85	2.8	2.92
^{172}Yb	75.79	51.1	9.11	18.1	19.41	18.88
^{175}Lu	10.66	6.99	0.9	3.02	2.94	2.98
^{206}Pb	11.32	3.07	b.d.l.	4.32	7.18	5.15
^{207}Pb	1.15	0.69	b.d.l.	0.67	0.83	0.74
^{208}Pb	b.d.l.	b.d.l.	b.d.l.	b.d.l.	b.d.l.	b.d.l.
^{232}Th	0.67	0.23	0.03	0.15	0.65	0.24
^{238}U	10.54	2.92	0.1	4.03	5.14	4.87

Chondrite normalised spider diagrams were used to highlight the differences in REE distribution among samples (Fig. 4). The mineralised sample EL18D18_113.8m has two distinct REE patterns (Groups 1 and 2). In Group 1 analyses (represented by the orange line), the REE patterns initially show an upward trend from La to Gd and preserve a strong Eu anomaly. The overall trend in heavy REEs (HREE) from Gd to Lu is downward, with a more pronounced decrease between Ho and Yb.

In Group 2 analyses (represented by the blue line) the REE patterns also show and initial upward trend from La to Gd and a strong Eu anomaly. However, this is followed by a marked decrease from Gd to Lu, with a particularly steep slope observed between Ho and Yb.

Analyses of apatite from the unmineralised sample EL18D18_123.0m (Group 3; represented by the green line), shows a relatively flat-lying, slightly upward convex trend from La to Sm and a strong Eu anomaly. There is an overall downward trend from Gd to Lu with a slightly concave upwards shape.

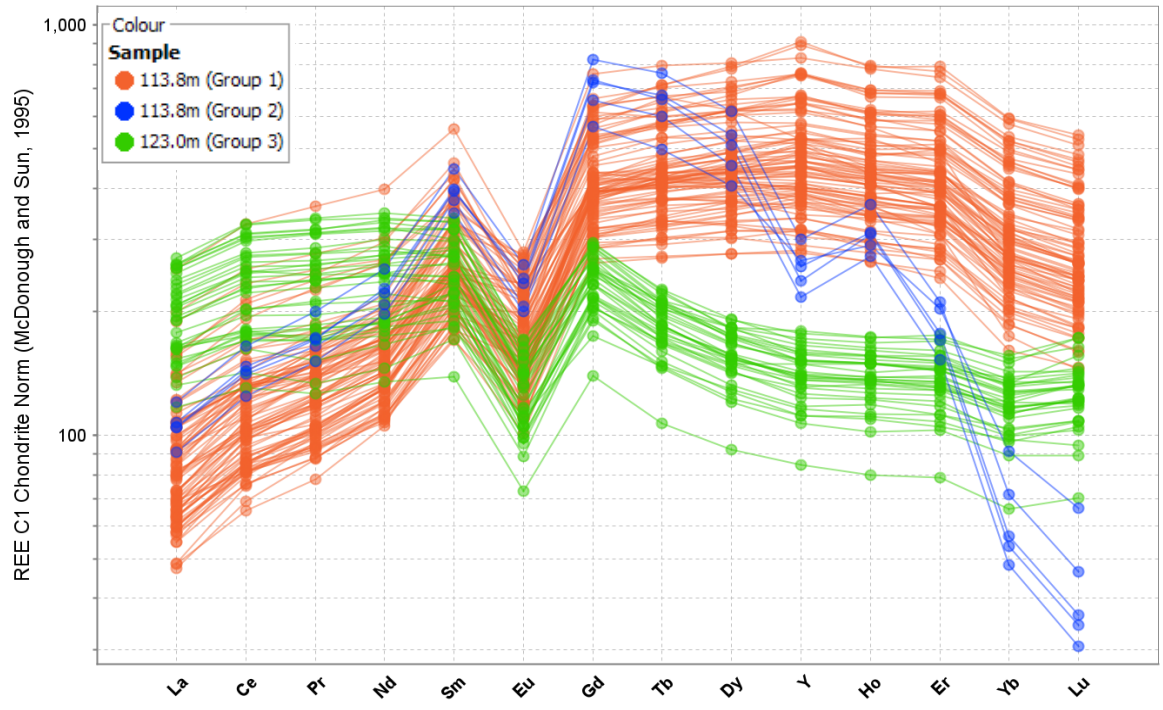

Figure 4. Chondrite normalised spider diagram showing the chemistry of apatite from drill hole EL18D18 at Jericho. Data from sample EL18D18_113.8m is shown in orange (Group 1) and blue (Group 2). Data from sample EL18D18_123.0m is shown in green (Group 3). See text for explanation of geochemical groupings. Drill hole location is shown in Figure 2. Chondrite normalised values refer to McDonough and Sun 1995.

The apatite data can be separated into distinct geochemical groups using La/Lu versus La/Sm ratios (Fig. 5). Group 1 apatite exhibit low La/Sm ratios, ranging from 0.2 to 0.5, with La/Lu ratios between 0.25 and 1.0. The clustering of these points indicates a depletion in light REEs (LREE) and enrichment in the HREEs. The Group 2 apatite have significantly higher La/Lu ratios, approximately between 1.25 and 3.5, while the La/Sm ratio is lower, around 0.25. This indicates enrichment of LREEs relative to HREEs, but strong depletion relative to the middle REEs (MREE). The La/Sm ratio in the Group 3 apatite is relatively high, ranging approximately

between 0.65 and 0.85, while the La/Lu ratio is primarily concentrated between 1.0 and 2.0. This suggests that these samples are relatively enriched in LREEs compared to the HREEs.

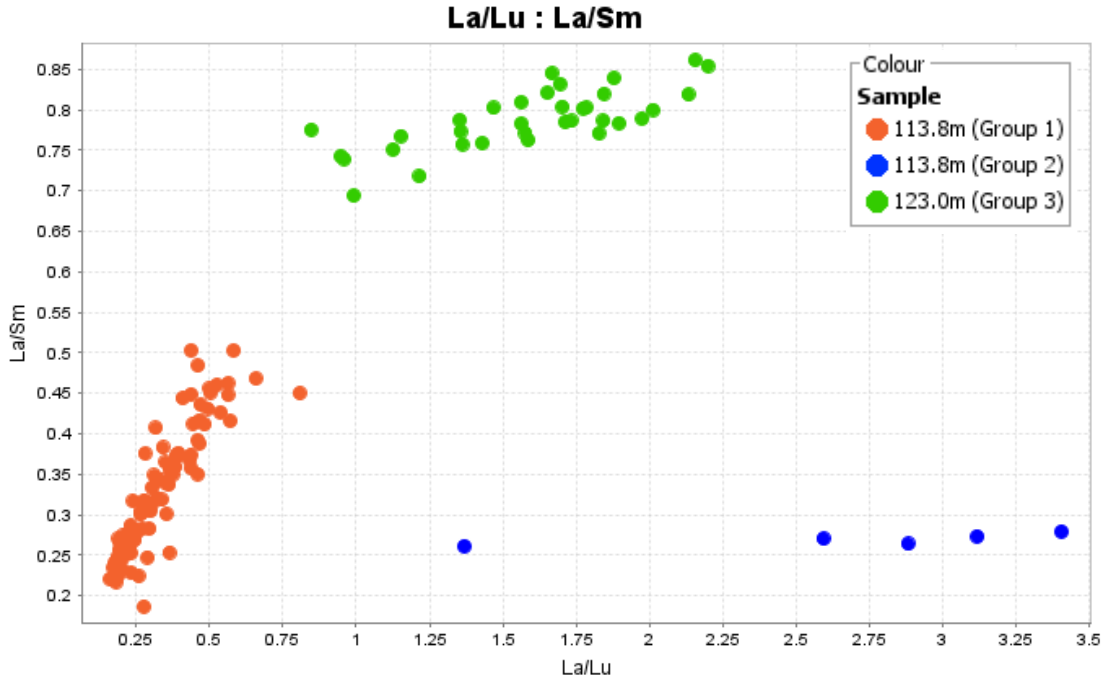

Figure 5. La/Lu versus La/Sm plot for analysed apatite from drillhole EL18D18. Apatite data is coloured according to the geochemical clusters identified from the REE chemistry (Fig. 4). Drill hole location is shown in Figure 2.

Box and whisker plots demonstrate the difference in chemistry between the three apatite groups (Fig. 6). All three apatite groups preserve similar concentrations of P (19.6 – 26.2 wt%) and Ca (38.5 – 42.9 wt%). Group 1 apatite have the lowest LREE concentrations (La, Ce, Pr, Nd, Sm), with the widest distribution and some outliers. Group 2 apatite preserve lower LREE concentrations with the most consistent and concentrated data distribution. The LREE concentrations in Group 3 apatite are variable and preserve the highest average concentration of all LREEs except Sm. For the MREEs (Eu, Gd, Tb, Dy) Group 2 apatite preserve the highest concentration with the least variability. Group 1 apatite have slightly lower concentrations but a broader distribution, and Group 3 apatite exhibits the lowest concentrations. The HREEs are not as consistent in concentration patterns. For the elements Ho, Er and Tm, Group 2 apatite shows relatively higher concentrations with a concentrated data distribution. Group 1 apatite preserves the highest concentration, while Group 3 apatite preserves the lowest concentrations, the widest distributions and greatest variability with some low-concentration outliers. Group 2 apatite preserve the lowers concentrations and most concentrated distribution for Yb, Lu, As, Th, U and Y. Group 1 apatite has the highest concentration and Group 3 apatite has a moderate concentration and an even distribution for these elements.

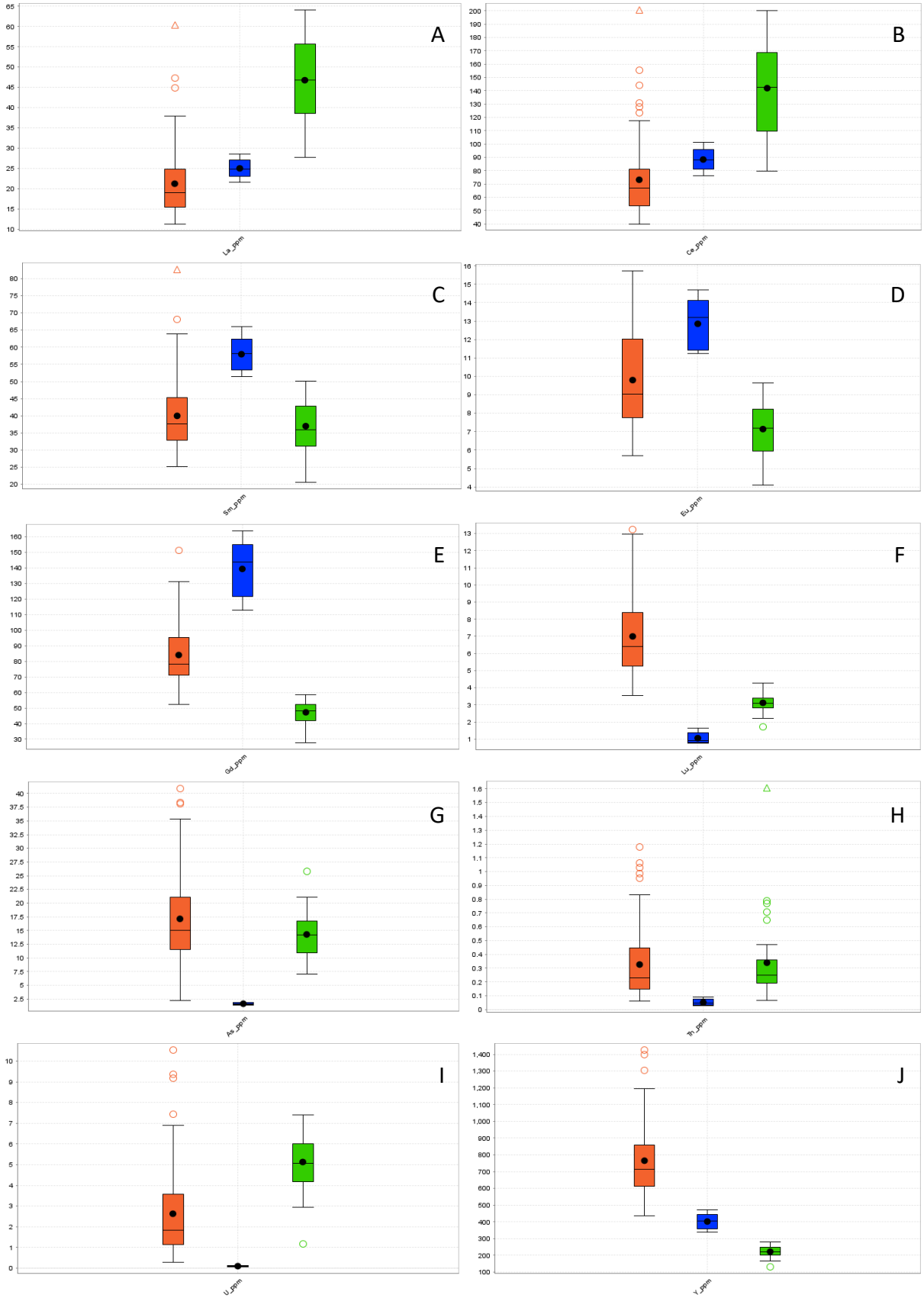

Figure 6. Box and whisker plots of trace element concentrations in ppm from selected LA-ICP-MS data for apatite samples used in this study, trace elements: La (A), Ce (B), Sm (C), Eu (D), Gd (E), Lu (F); As (G); Th (H); U (I); Y (J).

DISCUSSION

Source of apatite grains

Apatite trace and rare earth element (REE) chemistry has been shown to reflect the source of the apatite grains (e.g., Mao et al. 2016, Heinrichs et al., 2018, Zheng et al. 2022). Therefore, the trace and rare earth element chemistry of apatite grains from the Jericho area analysed in this study are compared with the published chemistry of apatite grains of known sources to determine their origin (Fig. 8; Heinrichs et al. 2018; Zheng et al. 2022). Group 1 and Group 3 apatite both mirror the chemistry of apatite from sedimentary rocks of different metamorphic grade (Fig. 8a, b, d, e). In particular, Group 1 apatite chemistry closely resembles the chemistry of amphibolite facies metamorphic rocks from the Grampian terrane in Scotland (Fig. 8a, d). Amphibolite facies metamorphic conditions mean the rock has been heated and buried to moderate temperatures and pressures. Group 3 apatite chemistry closely resembles the chemistry of greenschist to blueschist facies metamorphic rocks, also from the Grampian terrane in Scotland (Fig. 8c, e). These metamorphic conditions are lower temperatures and low to high pressure. The interpretation of the Group 1 and 3 apatite grains being of metamorphic origin and likely sourced from sedimentary rocks metamorphosed to greenschist to amphibolite conditions matches with what is seen in the Jericho area, which has been shown to have been metamorphosed to similar conditions (Little, 2021).

It is noted that the concentrations of LREEs in Group 1 (La, Ce, Pr, and Nd) are significantly lower than expected if they were fully consistent with those found in metamorphic grains (Fig. 8c, d). This apatite is from a mineralised sample. Given mineralisation at Jericho was associated with hydrothermal fluids (Batch et al., in Review), it can be assumed that the rock hosting the apatite has undergone alteration. Therefore, the differences in REE concentrations are possibly due to the alteration of apatite, induced by mineralising fluids, which would cause the apatite to undergo chemical changes, leading to the leaching of LREEs and the formation of rhabdophane. Evidence of this can be seen in Figure 2a, where a mineral with a bright BSE response is present encasing the apatite grain. This bright mineral is rhabdophane ($[La,Ce,Nd]PO_4 \cdot nH_2O$), a REE-bearing phosphate mineral, which has previously been identified at Jericho (Batch et al., in Review).

Metasomatism refers to the chemical alteration by a fluid, as described by Putnis and Austrheim (2010). Studies by Harlov et al. (2002) and Harlov et al. (2005) have shown significant differences in Ce and in apatite between unaltered and metasomatised, as observed through microprobe analysis. They show that Ce are markedly lower in the metasomatic regions compared to the unaltered apatite regions. This suggests that metasomatic processes can lead to a depletion of Ce concentrations, resulting in lower levels of LREEs in metasomatised regions compared to unaltered regions. Therefore, it is possible that the depleted LREE concentrations in Group 1 metamorphic apatite relative to Group 3 metamorphic apatite is due to alteration.

Group 2 apatite (Fig. 8c) show similar strongly concave upwards trace and rare earth element patterns to apatite seen in other areas of mineralisation, such as the Hatu orogenic Au deposit in northwest China (Fig. 8c, f). Differences between the two apatite groups may be attributed to them being sourced from different deposits, noting that no other apatite data is available from another ISCG deposit. Therefore, the similarity between the apatite data from the Hatu orogenic Au deposit and the Group 2 apatite data from Jericho is used here to suggest that

the Group 2 apatite grains are likely newly formed apatite that crystallised in a hydrothermal, mineralising environment.

Based on the analysis of apatite, it is reasonable to conclude that the Group 1 apatite grains from EL18D18_113.8m consist of metamorphic grains altered by mineralisation-associated hydrothermal fluids, and Group 2 apatite grains from the same sample consist of grains formed directly from the mineralisation-associated hydrothermal fluid. Group 3 apatite grains from EL18D18_123.0m consist of unaltered metamorphic grains.

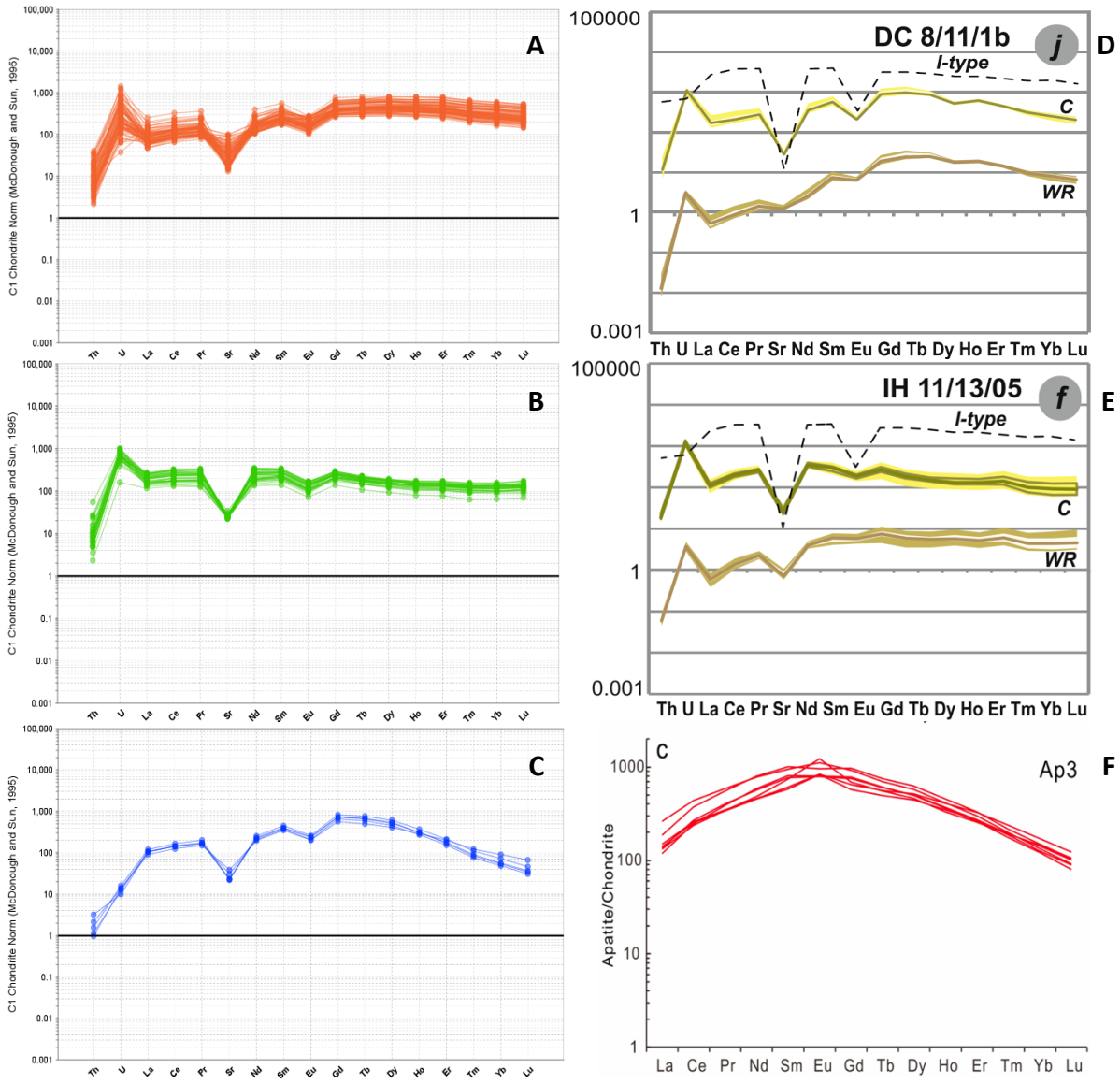

Figure 8. Chondrite normalised spider diagram showing the chemistry of apatite from drill hole EL18D18 at Jericho: (a) Group 1 apatite, mineralised sample EL18D18_113.8m; (b) Group 2 apatite, mineralised sample EL18D18_113.8m; (c) Group 3 apatite, unmineralised (barren) sample EL18D18_123.0m. (d-e) Chondrite-normalised trace element (labelled as C) and whole-rock normalised trace element (labelled as WR) plots for apatite from metapelites (metamorphosed sediments) from the Dalradian Supergroup of the Grampian terrane in Scotland and northwest Ireland. Dashed black line: reference for I-type granite..(d) Amphibolite facies foliated metapelite; (e) Upper greenschist to blueschist facies foliated metapelite. Taken from Heinrichs et al. (2018). (f) Chondrite-normalised spider diagram for apatite grains from the Hatu orogenic Au deposit, northwest China

showing characteristic enrichment in MREEs with weak positive Eu anomaly. Taken from Zheng et al. (2022).

Apatite exploration criteria

The identification of apatite grains at the Jericho ISCG deposit, where the chemistry is interpreted to indicate alteration due to hydrothermal activity associated with mineralization, suggests the potential to develop geochemical exploration criteria for ISCG deposits using apatite chemistry. These criteria would be best defined by the chemistry of Group 2 apatite, which is interpreted to be of hydrothermal origin and exhibits a distinctive chemistry different from that of Group 1 and Group 3 apatite, which are of metamorphic origin. The key distinguishing features of Group 2 apatite include a steep positive LREE slope and a steep negative HREE slope, which are clearly visible on the La/Lu versus La/Sm diagram (Fig. 5). Therefore, apatite with La/Lu ratios greater than 0.5 and La/Sm ratios less than 0.3 may be indicative of hydrothermal apatite associated with ISCG mineralization.

This approach holds significant potential, especially in the context of the global transition to renewable energy. As the demand for critical minerals continues to rise, the ability to accurately identify and exploit new mineral deposits becomes increasingly important. By advancing our knowledge of mineral chemistry and its application in exploration, this research not only contributes to scientific understanding but also supports practical efforts to secure the resources needed for a sustainable energy future.

Limitations

The study presents several limitations that warrant further investigation to fully understand the applicability of using apatite for ISCG exploration. The geochemical criteria proposed here require additional validation to confirm their effectiveness across different settings. While the association of apatite with ISCG mineralization at Jericho is inferred from its occurrence in samples containing sulfide minerals, direct petrographic evidence linking apatite with sulfide minerals remains elusive due to the nature of the mineral separates analysed. Moreover, apatite U-Pb geochronology could provide critical insights by correlating the timing of apatite growth with mineralization events in the Cloncurry region. Additionally, further research is needed to conclusively determine the origin of the apatite grains, including the potential for an igneous origin. Despite these limitations, this study introduces the possibility of using apatite chemistry as an indicator of ISCG mineralization, marking a novel approach in the field.

The study's implications extend beyond immediate mineral exploration. The specific patterns identified in apatite grains serve as a practical guide for geologists and mining companies, offering a method to narrow down potential sites for further investigation. By integrating these findings into exploration strategies, it becomes possible to improve the efficiency and accuracy of mineral prospecting, particularly in regions where traditional methods may be less effective. However, it is important to acknowledge the limitations of this study, particularly the relatively small sample size. This limitation suggests that while the findings are promising, they would benefit from further validation. Future research could expand the sample range, including a broader array of geological settings and mineral types, to ensure that the conclusions drawn here are robust and widely applicable.

CONCLUSIONS

This dissertation shows how apatite chemistry could potentially be used in exploration for iron sulfide-copper-gold deposits. Three chemical groups of apatite were identified from mineral chemistry analysis of samples taken from drill hole EL18D18. One sample was taken from within mineralisation (EL18D18_113.8m), and a second sample was taken from unmineralised (barren) rock (EL18D18_123.0m). Group 1 apatite grains from sample EL18D18_113.8m consist of metamorphic grains altered by mineralisation-associated hydrothermal fluids, and Group 2 apatite grains from the same sample consist of grains formed directly from the mineralisation-associated hydrothermal fluid. Group 3 apatite grains from sample EL18D18_123.0m consist of unaltered metamorphic grains.

The study highlights that the ratios of La/Sm versus La/Lu are key to identifying apatite associated with hydrothermal alteration and mineralization. Specifically, Group 2 apatite, interpreted to have a hydrothermal origin, shows a distinctive geochemical profile with a pronounced positive slope in LREE and a steep negative slope in HREE. These characteristics are evident on the La/Lu versus La/Sm diagram. Apatite with La/Lu ratios exceeding 0.5 and La/Sm ratios below 0.3 may indicate hydrothermal apatite linked to ISCG mineralization, distinguishing it from the metamorphic Group 1 and Group 3 apatite which display different rare earth element patterns.

These distinct alteration patterns observed across different groups of apatite grains not only shed light on the complex processes of mineralisation but also highlight the critical role of apatite in tracking hydrothermal activity. This understanding is crucial for guiding future exploration efforts, as it provides a reliable indicator of the conditions under which valuable mineral deposits may form.

ACKNOWLEDGEMENTS

This research was conducted as part of a MinEx CRC project. The author extends special thanks to Susie Ritch and Justin Payne for their invaluable assistance in obtaining the LA-ICP-MS results. Their support and expertise were crucial to the success of this study.

REFERENCES

Adlakha, E., et al. 2018. The origin of mineralizing hydrothermal fluids recorded in apatite chemistry at the Cantung W–Cu skarn deposit, NWT, Canada. European Journal of Mineralogy, 30(6), pp.1095-1113.

Andersson, S.S., et al. 2019. Apatite as a tracer of the source, chemistry and evolution of ore-forming fluids: The case of the Olserum-Djupedal REE-phosphate mineralisation, SE Sweden. Geochimica et Cosmochimica Acta, 255, pp.163-187.

Anika, O.C., et al. 2022. Prospects of low and zero-carbon renewable fuels in 1.5 degree net zero emission actualisation by 2050: A critical review. Carbon Capture Science & Technology, 5, p.100072.

Baker, T., 1998. Alteration, mineralization, and fluid evolution at the Eloise Cu-Au deposit, Cloncurry district, northwest Queensland, Australia. Economic Geology, 93(8), pp.1213-1236.

Batch, T., et al. in Review. REE-bearing phosphate mineral chemistry for iron sulfide-copper-gold exploration: A study at Jericho, NW Queensland, Australia.

Belousova, E.A., et al. 2002. Apatite as an indicator mineral for mineral exploration: Trace-element compositions and their relationship to host rock type. Journal of Geochemical Exploration, 76(1), pp.45-69.

Betts, P.G., et al. 2006. Synthesis of the Proterozoic evolution of the Mt Isa Inlier. Australian Journal of Earth Sciences, 53(1), pp.187-211.

Bouzari, F., et al. 2016. Hydrothermal alteration revealed by apatite luminescence and chemistry: A potential indicator mineral for exploring covered porphyry copper deposits. Economic Geology, 111(6), pp.1397-1410.

Brotodewo, A., et al. 2021. Recognising Mineral Deposits from Cover; A Case Study Using Zircon Chemistry in the Gawler Craton, South Australia. Minerals, 11(9), p.916.

Bruand, E., et al. 2017. Apatite trace element and isotope applications to petrogenesis and provenance. American Mineralogist, 102(1), pp.75-84.

Case, G., et al. 2018. Delineating the structural controls on the genesis of iron oxide–Cu–Au deposits through implicit modelling: a case study from the E1 Group, Cloncurry District, Australia. Geological Society, London, Special Publications, 453(1), pp.349-384.

Chen, B., et al. 2019. Pathways for sustainable energy transition. Journal of Cleaner Production, 228, pp.1564-1571.

Chew, D.M., et al. 2011. U–Pb and Th–Pb dating of apatite by LA-ICPMS. Chemical Geology, 280(1-2), pp.200-216.

Foster, D. R. W., and Rubenach, M. J., 2006, Isograd pattern and regional low pressure, high-temperature metamorphism of pelitic, mafic and calc-silicate rocks along an east – west section through the Mt Isa Inlier: Australian Journal of Earth Sciences, v. 53, p. 167-186.

Harlov, D.E., et al. 2002. Fluid-induced nucleation of (Y+ REE)-phosphate minerals within apatite: Nature and experiment. Part I. Chlorapatite. American Mineralogist, 87(2-3), pp.245-261.

Harlov, D.E., et al. 2005. An experimental study of dissolution–reprecipitation in fluorapatite: fluid infiltration and the formation of monazite. Contributions to Mineralogy and Petrology, 150, pp.268-286.

Henrichs, I.A., et al. 2018. The trace element and U-Pb systematics of metamorphic apatite. Chemical Geology, 483, pp.218-238.

Kelley, D.L., et al. 2006. Beyond the obvious limits of ore deposits: The use of mineralogical, geochemical, and biological features for the remote detection of mineralization. Economic Geology, 101(4), pp.729-752.

Little, G., 2021, Do we need to refine the existing geological and exploration models?, Mineral Systems of the Mount Isa Inlier: Mount Isa, EGRU.

Mao, M., et al. 2016. Apatite trace element compositions: A robust new tool for mineral exploration. Economic Geology, 111(5), pp.1187-1222.

McClenaghan, M.B., 2005. Indicator mineral methods in mineral exploration. Geochemistry: Exploration, Environment, Analysis, 5(3), pp.233-245.

McConnell, D., 2012. Apatite: its crystal chemistry, mineralogy, utilization, and geologic and biologic occurrences (Vol.5). Springer Science & Business Media.

McDonough, W.F. and Sun, S.S., 1995. The composition of the Earth. Chemical geology, 120(3-4), pp.223-253.

Minotaur Exploration, 2019, Jericho copper-gold discovery: What lurks beneath the deep blue sea, GSQ Technical Workshop.

Minotaur Exploration, 2020, Maiden Jericho resource and Cloncurry exploration update, ASX Release.

Mitsis, I. and Economou-Eliopoulos, M., 2001. Occurrence of apatite associated with magnetite in an ophiolite complex (Othrys), Greece. American Mineralogist, 86(10), pp.1143-1150.

Mudd, G.M. and Jowitt, S.M., 2018. Growing global copper resources, reserves and production: Discovery is not the only control on supply. Economic Geology, 113(6), pp.1235-1267.

Piccoli, P.M. and Candela, P.A., 2002. Apatite in igneous systems. Reviews in Mineralogy and Geochemistry, 48(1), pp.255-292.

Ptáček, P., 2016. Introduction to apatites. In Apatites and their Synthetic Analogues - Synthesis, Structure, Properties and Applications. IntechOpen.

Ptáček, P., 2016. Other Minerals from the Supergroup of Apatite. In Apatites and their Synthetic Analogues - Synthesis, Structure, Properties and Applications. IntechOpen.

Putnis, A. and Austrheim, H., 2010. Fluid-induced processes: Metasomatism and metamorphism. Geofluids, 10(1-2), pp.254-269.

Rakovan, J., 2002. Growth and surface properties of apatite. Reviews in Mineralogy and Geochemistry, 48(1), pp.51-86.

Rubenach, M.J., et al 2008. Age constraints on the tectonothermal evolution of the Selwyn Zone, Eastern fold belt, Mount Isa Inlier. Precambrian Research, 163(1-2), pp.81-107.

S&P Global, 2022. The Future of Copper: Will the looming supply gap short-circuit the energy transition? pp.15-17.

Simon, A.C., et al. 2018. Kiruna-type iron oxide-apatite (IOA) and iron oxide copper-gold (IOCG) deposits form by a combination of igneous and magmatic-hydrothermal processes: Evidence from the Chilean iron belt.

Thompson, R.L., Bank, T., Montross, S., Roth, E., Howard, B., Verba, C., and Granite, E., 2018. Analysis of rare earth elements in coal fly ash using laser ablation inductively coupled plasma mass spectrometry and scanning electron microscopy. Spectrochimica Acta Part B: Atomic Spectroscopy, 143, pp.1-11.

Thomson, S.N., et al. 2012. Routine low-damage apatite U-Pb dating using laser ablation–multicollector–ICPMS. Geochemistry, Geophysics, Geosystems, 13(2).

Tiddy, C., et al. 2021. Monazite as an Exploration Tool for Iron Oxide-Copper-Gold Mineralisation in the Gawler Craton, South Australia. Minerals, 11(8), p.809.

Walters, S. and Bailey, A., 1998. Geology and mineralization of the Cannington Ag-Pb-Zn deposit; an example of Broken Hill-type mineralization in the eastern succession, Mount Isa Inlier, Australia. Economic Geology, 93(8), pp.1307-1329.

Xie, F., et al. 2018. Apatite and zircon geochemistry of Jurassic porphyries in the Xiongcun district, southern Gangdese porphyry copper belt: Implications for petrogenesis and mineralization. Ore Geology Reviews, 96, pp.98-114.

Zhang, F., et al. 2020. Geochemical and isotopic study of metasomatic apatite: Implications for gold mineralization in Xindigou, northern China. Ore Geology Reviews, 127, p.103853.

Zheng, J., et al. 2022. Hydrothermal apatite record of ore-forming processes in the Hatu orogenic gold deposit, West Junggar, Northwest China. Contributions to Mineralogy and Petrology, 177(2), p.27.